Global Biogeochemical Cycles

RESEARCH ARTICLE
10.1029/2019GB006497

Resource Availability and Entrainment Are Driven by Offsets Between Nutriclines and Winter Mixed-Layer Depth

S. J. Rigby[1], R. G. Williams[1], E. P. Achterberg[2], and A. Tagliabue[1]

[1]Department of Earth, Ocean and Ecological Sciences, School of Environmental Science, University of Liverpool, UK, [2]GEOMAR Helmholtz Centre for Ocean Research Kiel, Kiel, Germany

Key Points:
- There are large scale regimes present in mixed-layer nutrient availability throughout the Atlantic Ocean
- Entrainment decreases the mixed layer availability of resources where the concentration decreases with depth
- Variations in nutrient availability and entrainment are linked to gradients in resource profiles combined with the depth of mixing

Supporting Information:
- Supporting Information S1

Correspondence to:
S. J. Rigby and A. Tagliabue,
s.j.rigby@liv.ac.uk;
a.tagliabue@liv.ac.uk

Citation:
Rigby, S. J., Williams, R. G., Achterberg, E. P., & Tagliabue, A. (2020). Resource availability and entrainment are driven by offsets between nutriclines and winter mixed-layer depth. *Global Biogeochemical Cycles*, *34*, e2019GB006497. https://doi.org/10.1029/2019GB006497

Received 10 DEC 2019
Accepted 22 APR 2020
Accepted article online 27 APR 2020

Abstract While phytoplankton play a key role in ocean biogeochemical cycles, the availability and supply pathways of resources that support their growth remain poorly constrained. Here, we show that the availability of various resources varies over several orders of magnitude throughout the Atlantic Ocean, causing regional contrasts in resource deficiency. Regional variations in the relative availability of nitrogen, phosphorous, silicon, iron, zinc, manganese, cobalt, and cadmium are important and result from the contrasts between winter mixing depths and differences in vertical profiles of the different resources. The winter-time thickening of the mixed layer may replenish or deplete resources via entrainment, depending on the vertical nutrient profile. For nutrients like nitrate, phosphate, and cadmium, entrainment is a consistent source term. While for others, such as manganese and iron, entrainment can reduce ocean resource availability, particularly in subtropical regions. Any future change to the depth of winter-time mixing will cause region-specific changes in relative availability of different resources that may have important ecological consequences.

1. Introduction

The growth and biomass accumulation of marine phytoplankton are key determinants of ocean biogeochemical cycles and the operation of the ocean carbon cycle. One key factor affecting the large scale distribution of marine phytoplankton in the sunlit upper ocean is the difference between the availability of nutrient and trace metal resources and biological demands (Martin & Fitzwater, 1988; Moore, 2016; Moore et al., 2013). Primary production and other cellular functions require a range of resources, including the macronutrients nitrogen (N), phosphorous (P), and silicon (Si, for diatoms and some dinoflagellates), as well as micronutrient trace metals such as iron (Fe), zinc (Zn), manganese (Mn), cadmium (Cd), and cobalt (Co; Falkowski et al., 1998; Ludwig & Matthews, 1997; Morel & Price, 2003; Prince & Morel, 1990; Rodionov et al., 2003; Sunda, 1989; Twining & Baines, 2013). The upper mixed layer is the key growth environment for marine phytoplankton and where biota thrive given sufficient resource availability. Changes in the resource supply are often invoked as a driver of variability in phytoplankton growth and primary production (Lampe et al., 2019; Marra et al., 1990; Okin et al., 2011).

The vertical profiles of different resources are known to vary both spatially and between resources (Tagliabue, 2019), driving large-scale patterns in availability of various resources (Moore, 2016). The shape of resource profiles is influenced by biogeochemical and physical processes. Biological consumption removes resources from the upper water column, organic particles then sink and resources are released back into the water column at depth through resupply processes such as remineralization (Twining et al., 2014). The combination of removal in surface waters and resupply at depths forms gradients in the vertical profiles of key resources, with the strongest vertical gradient known as the nutricline (Omand & Mahadevan, 2015; Tagliabue et al., 2014). The reservoir of resources below the nutricline is accessed by the seasonal deepening of the mixed layer. Thus, the relative positioning of multiple nutriclines determines the availability of different resources to phytoplankton. For instance, where the mixed layer extends below the N-nutricline (nitracline) but fails to access below the P-nutricline (phosphocline), the upper mixed layer will be enriched in N relative to P. We do not understand how spatial variations in upper ocean mixing depths and vertical resource profiles shape the availability of different resources on an ocean basin scale.

The availability of different resources is a crucial determinant of phytoplankton growth. Biological communities become deficient in a given resource if its availability is lower than the biological demand. In the Atlantic Ocean, high latitudes are considered as Fe deficient, low to mid-latitudes are N deficient, and the North Atlantic sub-tropical gyre as P deficient (Browning, Achterberg, Rapp, et al., 2017; Mills et al., 2004; Moore, 2016; Nielsdottir et al., 2009). Deficiency leads to limitation following biological consumption and is intensified if the resource supply to the growth environment is low in the deficient resource (Moore, 2016). For instance, using shipboard bioassay experiments in the South Atlantic, Browning, Achterberg, Rapp, et al. (2017) found that evidence of singular limitation (where one resource only limits), serial limitation (or secondary limitation, where a second resource becomes limiting after the supply of the first), or colimitation by Fe and N could be explained by the relative availability of N and Fe. Resource limitation is alleviated by the supply of the exhausted resource, irrespective of other resources; however, resource deficiency is reduced when the supply is abundant in the deficient resource relative to other resources. If the future ocean becomes more stratified (Bopp et al., 2001; Sen Gupta et al., 2009), with reduced upper ocean mixing depths, or mixed layers vary interannually (Holte et al., 2017), then any subsequent impact on the relative availability of resources may affect resource deficiency and biological communities.

Resources are delivered to the upper ocean via atmospheric processes and physical ocean processes. Lithogenic (Jickells et al., 2005) and anthropogenic (Conway et al., 2019) particles can be transported across the ocean by winds, then deposited at the air-sea interface via dry and wet deposition processes. A range of physical ocean processes transport dissolved resources to the upper ocean (Williams & Follows, 2003), such as upwelling (Oschlies, 2002), lateral advection (Williams et al., 2006), vertical turbulence (Martin et al., 2010), diapycnal mixing (Tuerena et al., 2019), diapycnal diffusion (Painter et al., 2014; Rijkenberg et al., 2012), and eddies (Conway et al., 2018). Here, we focus on the role of deep winter mixing since the entrainment of underlying waters has been shown to be fundamental in the delivery of resources to mixed-layer phytoplankton (Achterberg et al., 2018; Tagliabue et al., 2014; Williams et al., 2000).

Resource availability is altered by entrainment redistributing thermocline waters throughout the seasonal mixed layer. Underlying thermocline waters can be rich in a given resource due to resupply processes; however, these waters can also be deplete in a given resource due to interior ocean removal processes such as particle scavenging. The magnitude of the entrainment input to the mixed layer is determined by the volume of water entrained and the contrast in resource concentration from the mixed layer to underlying waters (Williams et al., 2000). Therefore, variability in the entrainment flux will likely occur in response to spatial variation in resource profiles and the depth of seasonal mixing.

Here, we use observations of multiple resources and their vertical profiles to explore basin scale patterns of resource availability in the mixed layer. Differences in resource availability are attributed to offsets in vertical profiles between each resource, most important is the depth of the nutricline. The *GEOTRACES* program has delivered a wealth of observations which reveal the array of vertical resource profiles present in the Atlantic Ocean, permitting a large scale analysis of entrainment for multiple resources (Schlitzer et al., 2018). We analyze the role of entrainment in either delivering or diluting resources in the seasonal mixed layer and the subsequent effect on resource availability. Finally, we speculate on changes to mixed-layer resource availability in a warmer climate and the future role of entrainment in biogeochemical cycling.

2. Methods

2.1. Data Sets

Observational data of nitrate (NO_3), phosphate (PO_4), Si, Fe, Zn, Mn, Cd, and Co were extracted from the 2017 *GEOTRACES* Intermediate Data Product (Schlitzer et al., 2018). Only *GEOTRACES* datapoints with "good" data quality flags were included (Figure 1). Monthly mean temperature, salinity, and mixed-layer depths were extracted from the 1° × 1° resolution *ECCO* circulation model (version 4, release 3), full period 1992–2015 (Figure 1 and Figure S1 in the supporting information; Forget et al., 2015; Fukumori et al., 2017).

Vertical profiles are presented in Longhurst Provinces (Longhurst, 2007), where 21 provinces were aggregated into five provinces throughout the Atlantic based on underlying biogeochemistry (Figure S2). The North Atlantic subpolar gyre (capped at 65°N due to data limitations) is composed of the Atlantic Arctic,

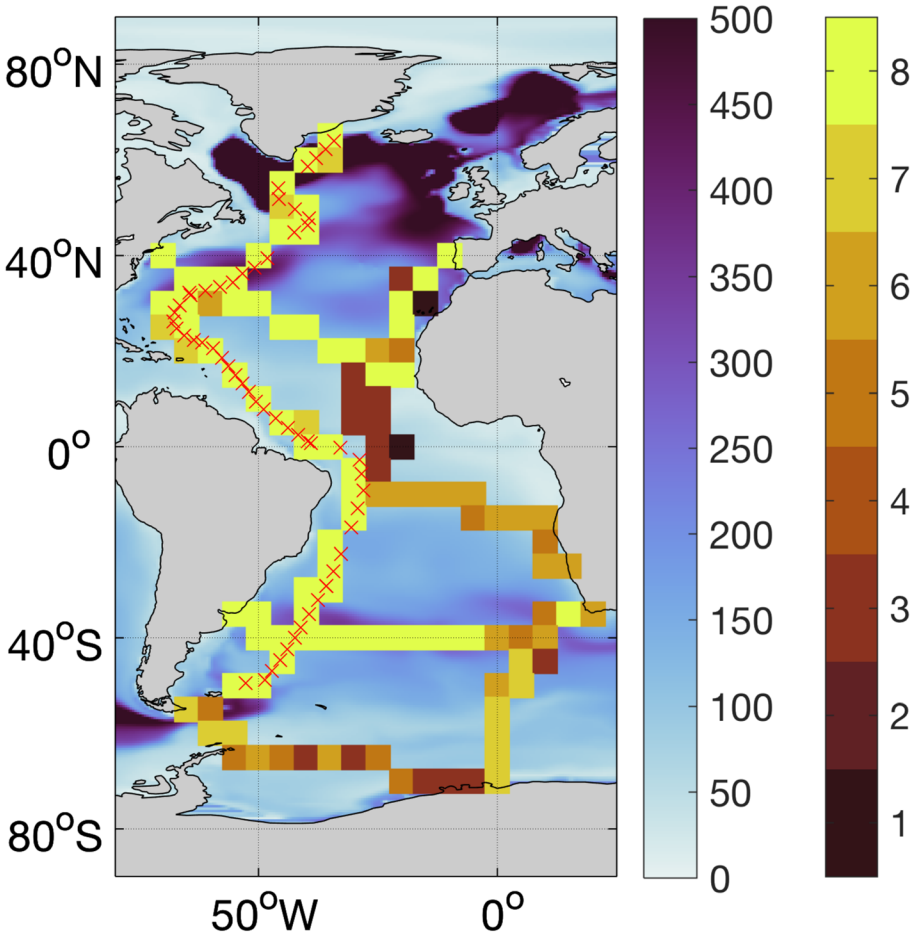

Figure 1. Monthly mean maximum mixed-layer depth (white–purple, in m) for the period 1992–2015 as reported in Estimating the Climate and Circulation of the Ocean version 4 release 3 (Forget et al., 2015; Fukumori et al., 2017). Overlaid, maximum number of observations (brown–yellow) available at a single station in 5 × 5 degree grid cells (from nitrate, phosphate, silica, iron, zinc, manganese, cadmium, and cobalt), biogeochemical data from the 2017 *GEOTRACES* Intermediate Data Product (Schlitzer et al., 2018). Stations associated with the *GEOTRACES GA02* cruise are indicated with red crosses.

Atlantic Subarctic, Northwest Atlantic Shelves (North of 45°N), and North Atlantic Drift provinces. The North Atlantic subtropical gyre is composed of North Atlantic Subtropical Gyral, Gulf Stream, and Northwest Atlantic (South of 45°N) provinces. The equatorial Atlantic is composed of the Caribbean, North Atlantic Tropical Gyral, Eastern (Canary) Coastal, Western Tropical Atlantic Eastern Topical Atlantic, Guinea Current Coastal, and Guianas Coastal provinces. The South Atlantic subtropical gyre province is composed of the Brazil Current Coastal, South Atlantic Gyral, and Benguela Current Coastal provinces. The Southern Ocean province is composed of the Southwest Atlantic Shelves, South Subtropical Convergence, Subantarctic Water Ring, Antarctic, and Austral Polar provinces. This aggregated province approach better suits the limited spatial distribution of shipboard measurements available from *GEOTRACES*. The nutricline for each resource is defined as the depth in the upper 500 m where the gradient of a given resource is maximum ($d[R]/dz_{max}$, where [R] is a resource concentration and z is depth).

2.2. Winter Mixed-Layer Resource Availability

Due to the spatial and temporal limitations of the observational *GEOTRACES* data set, monthly profiles of each resource were constructed using temperature and salinity derived density profiles from *ECCO*. Density is calculated at each location in the *GEOTRACES* data set from shipboard temperature and salinity observations. On a profile-by-profile basis, the observational relationship between density and each resource was

applied to monthly density structures at the corresponding latitude and longitude. This approach assumes resource concentrations are conserved on isopycnals, meaning biogeochemical processes are invariable from the time of observation through to winter.

The winter mixed-layer resource availability is calculated by integrating reconstructed winter resource profiles from the surface to the maximum annual mixed-layer depth reported in the *ECCO* model, equation (1).

$$Resource\ Stock\ \left(mol\ m^{-2}\right) = \int_{z=H}^{z=0} [R(z)]\ dz, \tag{1}$$

where z is depth, H is mixed-layer thickness, and R is a given resource concentration. Vertical profiles were required to contain a minimum of two observations in the mixed layer. Profiles were linearly interpolated to meter resolution. The mean value of measurements was taken where multiple observations were available within 1 m. From the surface to the shallowest observation, resource concentrations were set to equal the shallowest observation. Resource concentrations were set to zero where concentrations were below zero as a feature of interpolation.

2.3. Entrainment Calculation

The entrainment flux is diagnosed from equation (2) using the mixed-layer thickening and nutrient profiles on a monthly timescale (Williams et al., 2000).

$$Entrainment\ \left(mol\ m^{-2}\ s^{-1}\right) = \frac{1}{T}\int_{0}^{year} \Lambda\ \left([R(t)]_{th} - [R(t)]_{ml}\right)\frac{dH}{dt}dt, \tag{2}$$

where T represents 1 year (months), $[R(t)]_{th}$ is the thermocline mean concentration of a resource R (mol m^{-3}) in month t, $[R(t)]_{ml}$ is the mixed layer mean concentration of resource N (mol m^{-3}) in month t and Λ is the Heaviside function as defined by Kraus and Turner (1967), where

$$\Lambda \equiv \Lambda\left(\frac{dH}{dt}\right) = \begin{matrix} 1 \\ 0 \end{matrix}\ for \frac{dH}{dt} \gtrless 0. \tag{3}$$

Entrainment occurs when the mixed layer deepens, such as in winter or due to enhanced convection in other seasons (e.g., storms in summer).

3. Results

3.1. Upper Ocean Resource Profiles

The vertical profile of a given resource reflects the resource availability throughout the water column (Figures 2 and S3). Any differences between the vertical profiles of individual resources may be caused by differences in their associated biogeochemical cycles. Further, there is a spatial variability in the vertical profiles of a single resource due to regional variations in the underlying processes.

3.1.1. Nutrient Type Profiles

Nutrient-type resources, such as NO_3, PO_4, Si, Cd, and Zn display a consistent depletion at the surface due to biological uptake, which is accompanied by increasing concentrations with depth due to either the resupply from the remineralization of sinking particles (Tagliabue, 2019) or the transport of nutrient-rich deep water which has received particles upstream (Middag et al., 2018, 2019).

NO_3 and PO_4 display a nutrient-type profile throughout the Atlantic as concentrations increase with depth in all provinces (Figures 2a and 2b; Rijkenberg et al., 2014; Tuerena et al., 2015). The Atlantic Ocean median surface NO_3 and PO_4 concentrations are 12 and 0.6 μmol kg^{-1}, increasing to 28 and 2 μmol kg^{-1}, respectively, at a depth of 500 m (Figure 2a). There is complete surface depletion in the North Atlantic subtropical gyre, equatorial Atlantic, and South Atlantic gyre, where NO_3 concentrations are below detection limits. However, in the Atlantic subpolar gyre and Southern Ocean, surface NO_3 stocks are not fully exhausted. The Atlantic lower quartile is near zero at the surface, meaning at least 25% of the Atlantic surface observations are deplete in NO_3. The depth at which NO_3 concentrations increase ranges from around 40 m in the North Atlantic subtropical gyre to around 100 m in the equatorial Atlantic. Although many of these features are similar for PO_4, there are some key differences in their distributions (Figure 2b). For instance, the

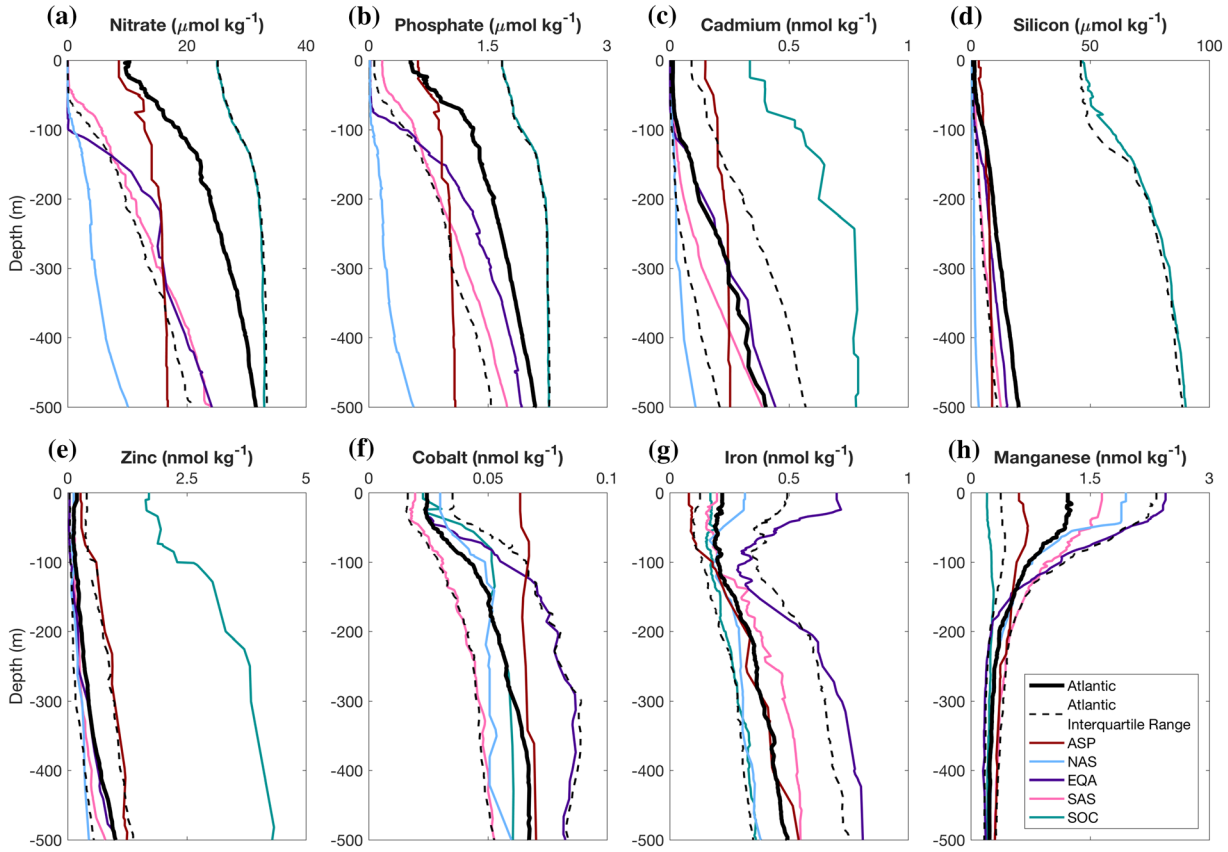

Figure 2. Vertical profiles of multiple elements in the Atlantic Ocean, median (black) and lower quartile and upper quartile (dashed black). Separated into biogeochemical provinces: Atlantic sub-polar gyre (ASP), North Atlantic subtropical gyre (NAS), equatorial Atlantic (EQA), South Atlantic subtropical gyre (SAS), and the Southern Ocean (SOC). Interquartile range for each nutrient in each province is provided in Figure S3. Data from the 2017 *GEOTRACES* Intermediate Data Product (Schlitzer et al., 2018).

Atlantic lower-quartile PO_4 concentration remains greater than zero throughout the water column, meaning less than 25% of observations are deplete in PO_4. Further, in the equatorial Atlantic, the depth at which concentrations increase is around 25 m shallower for PO_4 than NO_3.

The distribution of Cd is similar to that of macronutrients NO_3 and PO_4 (Figure 2c; Boye et al., 2012; Conway & John, 2015; Middag et al., 2019). Cd increases from near zero values in the surface to appreciable concentrations at 500 m, typical of a nutrient-type profile. In the low latitude provinces, Cd concentrations are depleted from the surface to ~100 m depth. Similar to NO_3 and PO_4, the median surface ocean concentration of Cd is only greater than zero in the high latitude provinces, where surface stocks are not fully exhausted. The accumulation of Cd in low latitudes tends to occur deeper in the water column than that of NO_3 and PO_4. The increase in Cd concentration at depth is largest in the equatorial Atlantic and weakest in the North Atlantic subtropical gyre. The greatest Cd concentrations are located in the Southern Ocean, which are approximately one order of magnitude larger than those in the North Atlantic subtropical gyre where the lowest Cd concentrations are found. In high latitudes, the vertical structure of Cd shows little variation between 250 and 500 m compared to the mid-low latitude provinces.

The vertical profile of Si also follows a nutrient-type profile (Figure 2d; Conway & John, 2014; Middag et al., 2019). The Atlantic median Si profile increases from near zero in the surface to 18 μmol kg^{-1} at 500 m depth. Si concentrations are below detection limits in the South Atlantic subtropical gyre and equatorial Atlantic. Surface depletion of Si occurs in all provinces as surface concentrations are lower than those at depth. The lowest water column Si concentrations are located at the surface in the North Atlantic subtropical gyre, where Si concentrations show the weakest vertical increase. The largest increase in Si from the surface to 500 m occurs in the equatorial Atlantic, due to the influence of Si-rich waters laterally

transported from the Southern Ocean (Sarmiento et al., 2004). Si concentrations are an order of magnitude higher in the Southern Ocean than any other province. Si accumulates deeper in the water column than NO_3 and PO_4 due to the noted longer regeneration length scale of Si (Holzer et al., 2014),

The broad distribution of Zn is known to be similar to Si, with both exhibiting a nutrient-type profile (Figure 2e; Conway & John, 2014; Croot et al., 2011; Wyatt et al., 2014). In general, Zn stocks are depleted in the upper waters relative to those at depth and then increase to 500 m depth, with the largest Zn concentrations at each depth level found in the Southern Ocean. There is little increase in either Si or Zn concentrations vertically due to the large remineralization length scale of both resources (Bruland, 1980; Weber et al., 2018). There are some differences in the vertical profiles of Si and Zn, with subsurface minima in Zn profiles (e.g., in the tropics) and a smaller increase in Zn with depth than Si in the Atlantic subpolar gyre.

3.1.2. Hybrid and Scavenged Profiles

Hybrid resources, such as Fe and Co, display a combination of both nutrient-type and scavenged-type characteristics (Tagliabue, 2019). Hybrid profiles are typically depleted at the surface due to biological uptake and concentrations increase with depth due to remineralization before decreasing again as scavenging becomes dominant. Scavenged-type resources, such as Mn, exhibit a surface maxima, usually due to resource inputs, followed by an exponential decline with depth due to scavenging onto sinking particles.

Co displays a hybrid profile throughout the Atlantic, exhibiting a nutrient-type profile above ~500 m and scavenged-type profile deeper in the water column (Dulaquais et al., 2014; Noble et al., 2012). The Atlantic median Co profile shows concentrations are low in the upper 20 m and increase with depth over the upper 500 m, indicative of a nutrient-type profile (Figure 2f). Incomplete surface depletion of Co (relative to 100–500 m) occurs in each province, excluding the Atlantic subpolar gyre. In the Atlantic subpolar gyre, Co shows little variation with depth compared to other provinces. The highest Co concentrations are located in the equatorial Atlantic at a subsurface maxima (0.08 nmol kg^{-1}) at 300 m. The vertical profile of Co in the South Atlantic gyre displays a decrease in Co concentration to a subsurface minima at 40 m. Overall, there is little large-scale spatial variability in the vertical distribution of Co as median Co concentrations reported for each individual province fall between the full Atlantic interquartile range (excluding the upper 100 m in the Atlantic subpolar gyre).

Fe shows a mix of both scavenged-type and nutrient-type behavior in different regions (Figure 2g; Hatta et al., 2015; Klunder et al., 2011; Rijkenberg et al., 2014). There is a surface depletion of Fe in the Atlantic subpolar gyre and Southern Ocean, likely due to biological consumption and the lack of dust input at the air-sea interface. Conversely, in the North Atlantic subtropical gyre, equatorial Atlantic and South Atlantic gyre, the surface ocean is moderately enriched in Fe. Surface maxima due to dust inputs (Shelley et al., 2018) and subsurface minima in response to consumption at the subsurface chlorophyll maximum (Twining et al., 2015) are present in the North Atlantic subtropical gyre and equatorial Atlantic, indicative of a scavenged-type resource. However, below 100 m, Fe expresses consistent nutrient-type behavior in all provinces as concentrations increase due to the remineralization of sinking particles.

Mn shows a generally scavenged profile (Figure 2h), with a clear surface enrichment in all provinces, excluding the Southern Ocean (Boye et al., 2012; Middag et al., 2011; Noble et al., 2012). The median vertical profile of Mn decreases from surface maxima to a consistent lower level of around 0.2 nmol kg^{-1} at 500 m. Elevated surface stocks are most apparent in the equatorial Atlantic. Across the low latitude regions, dust inputs and the photochemical reduction of manganese oxides to soluble dissolved Mn (II) causes elevated surface concentrations which then decrease vertically (Jickells et al., 2005; Shelley et al., 2018; van Hulten et al., 2017). The lowest Mn concentrations are located in the Southern Ocean, where the Mn concentration remains relatively uniform over the upper 500 m.

3.2. Vertical Position of Nutriclines

In the following, we focus on the western Atlantic *GEOTRACES* section (GA02, Figure 1) to examine how nutricline depths vary as a function of latitude across different resources (Figure 3). Detailed maps of nutricline depths and offsets between the nutricline depth and winter mixed-layer depth are referred to below and available in Figures 4, S4, and S5.

There is a clear latitudinal structure in the depth of the nitracline, phosphocline, and Cd-nutricline along the GA02 meridional section (Figure 3a). For each resource, the nutricline undulates systematically between the

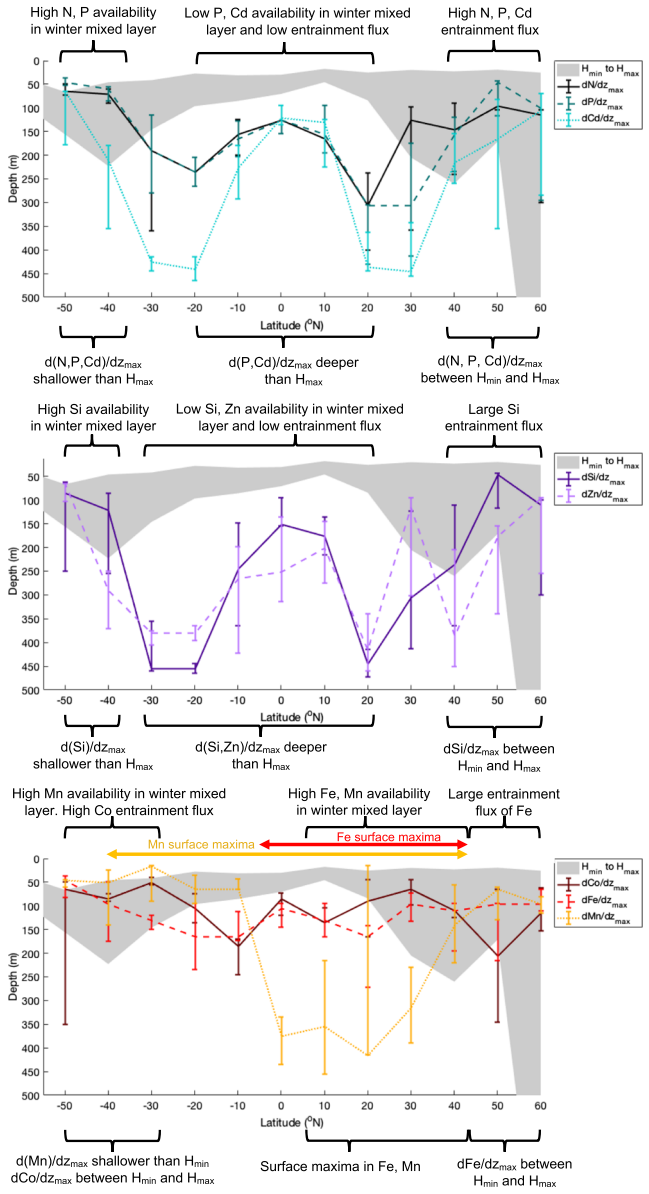

Figure 3. Depths of the (a) nitracline (dN/dz_{max}, black solid line), phosphocline (dP/dz_{max}, dark green dashed line), Cd-nutricline (dCd/dz_{max}, turquoise dotted line); (b) Si-nutricline (dSi/dz_{max}, purple solid line), Zn-nutricline (dZn/dz_{max}, pink dashed line) and (c) Co-nutricline (dCo/dz_{max}, maroon solid line), ferricline (dFe/dz_{max}, dashed red line) and Mn-nutricline (dMn/dz_{max}, yellow dotted line). Shaded region is the depth over which water is entrained into the mixed layer from the minimum mixed-layer thickness, H_{min}, to the maximum mixed-layer thickness in winter, H_{max}. Nutricline depths, H_{min} and H_{max} are 10° zonal median values from Atlantic Ocean observations. Physical model data from ECCOv4r3 (Forget et al., 2015; Fukumori et al., 2017). Errorbars represent upper and lower quartile nutricline depths in each 10° zonal limit. Biogeochemical data from the western Atlantic (*GA02*) *GEOTRACES* cruise, (indicated in Figure 1) available in the 2017 *GEOTRACES* Intermediate Data Product (Schlitzer et al., 2018).

poles and the equator, being deepest in the subtropical gyres and shallowest in the Southern Ocean, North Atlantic and Equatorial Atlantic. The deepening of nutriclines in the subtropical gyres is particularly pronounced for Cd, which can be twice as deep as NO_3 and PO_4, while the phosphocline is deeper than the nitracline only in the low PO_4 north Atlantic subtropical gyre. It is only south of 40°S and north of 40°N that the winter mixed-layer depth is deeper than all three nutriclines, indicating high mixed-layer stocks and a large potential for entrainment inputs.

The Si- and Zn-nutriclines show a similar large-scale pattern to the nitracline and phosphocline along GA02 (Figure 3b). However, the latitudinal undulations in the Si and Zn nutriclines are around two-fold more pronounced, likely due to the noted longer remineralization length scale of Si and Zn (Holzer et al., 2014; Weber et al., 2018). The Si- and Zn-nutriclines are deeper than the winter mixed-layer depth from 30°S to 30°N, indicating low mixed-layer stocks and small entrainment inputs in this latitude band, while the Zn-nutricline is only shallower than the winter mixed-layer depth in high latitudes and at 30°N. As a consequence, the winter-mixed layer is replete in both Si and Zn at high latitudes only.

The latitudinal structures of the Co-nutricline, ferricline, and Mn-nutricline are notably different to those of nutrient-type resources (Figure 3c). Their large-scale patterns show little variation in the depths of the Co nutricline and ferricline, which do not extend below 200 m. The Mn nutricline does not extend below 200 m in the South Atlantic; however, in the subtropical North Atlantic, the Mn nutricline extends to ~400 m before shoaling towards the subpolar gyre. From 50°S to 30°S and north of 40°N, each nutricline resides above the winter mixed-layer depth, meaning mixed-layer resource stocks are replenished in winter months. At low latitudes, the nutricline of each resource is deeper than the depth attained by winter mixing, driving low mixed-layer resource stocks of Co, Fe, and Mn. However, surface maxima are present in the vertical profiles of Fe and Mn causing high mixed-layer Fe and Mn stocks (Figures 2g and 2h).

The offset between the winter-mixed layer and nutricline depth varies strongly with latitude, evidenced by the meridional *GEOTRACES* transect *GA02* along the western margin (Figures 1 and 3). However, there are also notable longitudinal variations (Figures 4 and S5). For example, from west to east in the tropical South Atlantic, observations move into the Benguela upwelling zone, which causes the NO_3-, PO_4-, and Si-nutricline to shallow by ~100 m (Figures S4a, S4b, and S4d). Unlike the western side of the basin, the winter mixed-layer nears the NO_3-, PO_4-, and Si- nutriclines within the Benguela upwelling region (Figures 4a, S5a, and S5c). This transition across the tropical South Atlantic is reversed when considering Mn, which has a deeper nutricline within the Benguela upwelling (Figure S5f). We find a further transition along 40°S, where the mixed layer penetrates ~250 m deeper than the NO_3-, PO_4-, Co-, and Mn-nutriclines in the open ocean. However, the offset is reduced to ~50 m towards coastal regions (Figures 5a, S5a, S5e, and S5f). In contrast, longitudinal changes in the nutricline depth and offsets with the mixed-layer depth are less apparent in the subtropical North Atlantic. In the Southern Ocean, south of 50°S, the ferricline resides below the winter mixed-layer depth, meaning that there is low Fe in the mixed layer and little Fe input from winter-time mixing (Figure 4b). The general pattern in the ferricline depth shows relatively little spatial structure in absolute depth (Figure S4g), but is known to be well structured in an isopycnal context (Tagliabue et al., 2014).

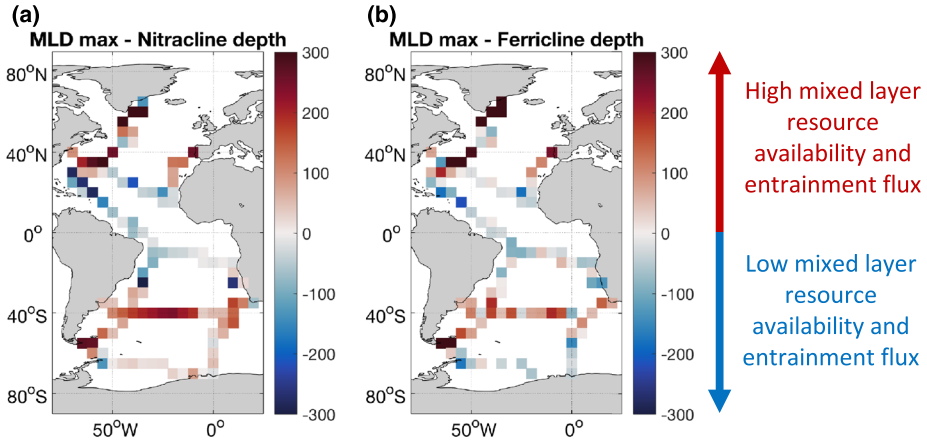

Figure 4. Difference (m) between the maximum mixed-layer depth (MLD max) and the nutricline depth ($d[N]/dz_{max}$, where [N] is the concentration of a given resource) for (a) nitrate and (b) iron. Biogeochemical data from the 2017 *GEOTRACES* Intermediate data product (Schlitzer et al., 2018), Mixed-layer depth defined by ECCOv4b (Forget et al., 2015; Fukumori et al., 2017).

3.3. Mixed-Layer Resource Availability

The winter mixed-layer depth varies throughout the Atlantic Ocean, from up to ~1,000 m at high latitudes to ~30 m in the subtropical South Atlantic (Figure 1). The winter mixed-layer depth coupled with the vertical distributions of each resource governs the basin-scale patterns in resource availability (Figure 5). Due to the challenges presented by ocean sampling during winter, particularly in the harsh Southern Ocean,

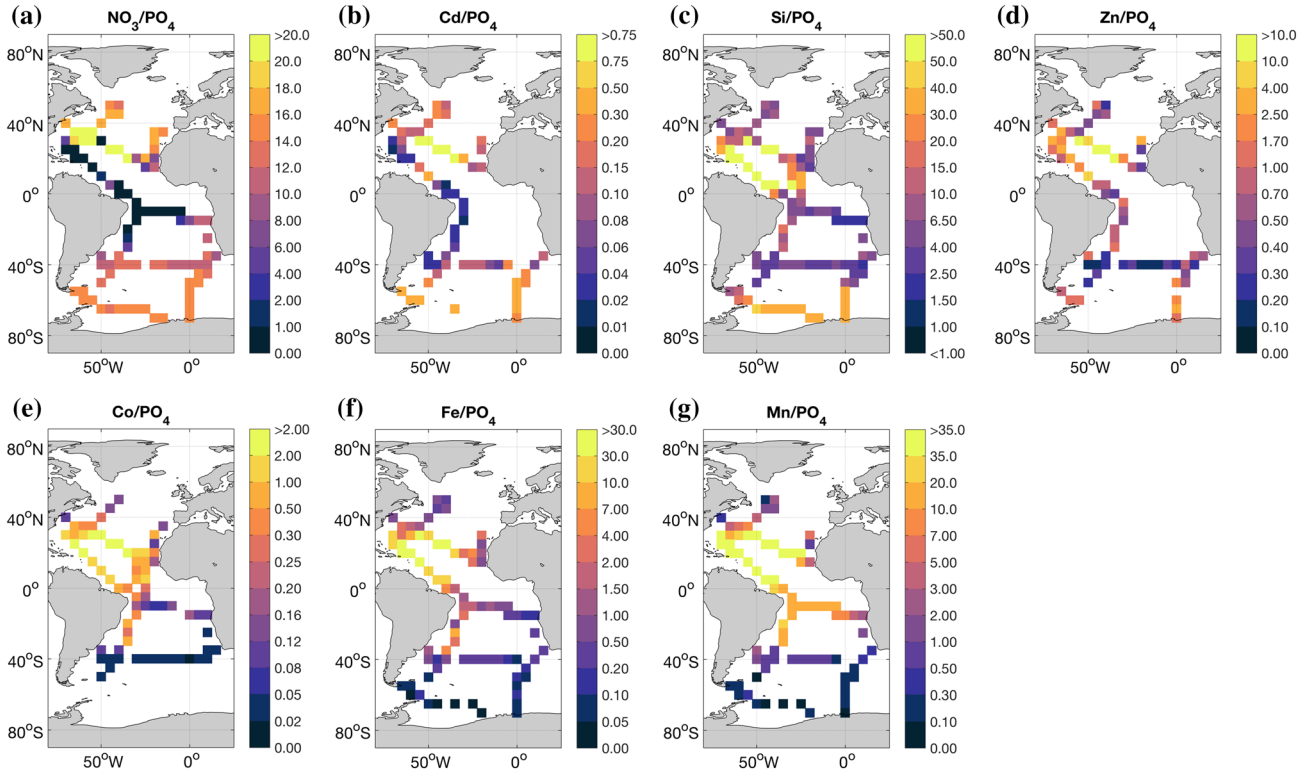

Figure 5. Resource ratios of depth integrated profiles obtained from the *GEOTRACES* 2017 IDP (Schlitzer et al., 2018). Ordered by nutrient type to scavenged type resource (see text). Profiles integrated to the maximum depth reached by the mixed layer over 1 year, as defined by ECCOv4r3 (Forget et al., 2015; Fukumori et al., 2017). (a, c) mol mol^{-1}, (b, e–g) mmol mol^{-1}. Calculations were completed on a profile by profile basis, displayed in 5 × 5 degree bins and median reported.

observations of resource concentrations contemporaneous with the winter mixed-layer depth are not often available. Observed resource profiles are projected to the time of the deepest mixed layer by assuming there is no loss to below the winter mixed layer. Biological uptake and subsequent remineralization effectively redistribute resources within the winter mixed layer; however, the integrated stock of a given resource in the winter mixed layer remains unchanged. The patterns we describe here are robust when resource stoichiometry is recalculated relative to NO_3 instead of PO_4 (Figure S6).

3.3.1. NO_3/PO_4 and Cd/PO_4

Generally, the availability of NO_3, relative to PO_4, is high in subpolar regions and lowest in the tropics, with enhanced NO_3 levels relative to PO_4 in upwelling regions (Figure 5a). The principle driver in the latitudinal structure observed is the relationship between the nitracline, phosphocline, and the winter mixed-layer depth (Figures 3a, 4a, and S5a). For instance, in the North Atlantic subpolar gyre, the deep mixed layers are able to access large subsurface NO_3 and PO_4 stocks resulting in substantial reserves of the two macronutrients in the mixed layer. In the Southern Ocean and North Atlantic, high standing stocks of NO_3 and PO_4 cause a near Redfield NO_3/PO_4 value (Redfield, 1934), irrespective of the mixed-layer depth. Spatial transitions in NO_3/PO_4 occur as the respective nutriclines shift position in the water column relative to the mixed-layer depth, exemplified in the tropical latitudes south of the equator where NO_3/PO_4 is higher in the east (10.9) and lower in the west (0.3; Figures 4a, 5a, and S5a). Cd/PO_4 shows a broadly similar distribution to NO_3/PO_4, driven by similarities in their vertical profiles (Figures 2a and 2c).

3.3.2. Si/PO_4 and Zn/PO_4

Si/PO_4 and Zn/PO_4 are broadly comparable to the nutrient-type distribution of NO_3/PO_4, as the Southern Ocean is replete in both Si and Zn and both elements are scarce at low latitudes (Figures 5c and 5d). Like NO_3/PO_4, elevated Si/PO_4 and Zn/PO_4 conditions found in the Southern Ocean are induced by high Si standing stocks in upper waters which are supplied by the upwelling of nutrient-rich deep waters (Figures 2d, 2e, S5c, and S5d). Severe depletion of PO_4 in the subtropical North Atlantic means that both Si/PO_4 and Zn/PO_4 are greatest here, despite low Si and Zn standing stocks compared to the Southern Ocean. The distribution of Zn/PO_4 is similar to that of Si/PO_4 (Figures 5d and 5e).

3.3.3. Co/PO_4, Fe/PO_4, and Mn/PO_4

The large-scale distributions of Co/PO_4, Fe/PO_4, and Mn/PO_4 are different to those resources that have a nutrient-type distribution (Figures 5e–5g). High latitudes are depleted in Co, Fe, and Mn relative to PO_4, while low latitudes are at least five-fold more replete in Co, Fe, and Mn. Dust input and low standing stocks of nutrient-like elements drive elevated availability of Co, Fe, and Mn at low latitudes. Co stocks may be enhanced where mixed layers overlay oxygen depleted zones due to the greater residence time of dissolved Co in low oxygen conditions (Hawco et al., 2016; Tagliabue et al., 2018). In the Southern Ocean, subsurface Fe stocks are deeper than winter mixing levels (Tagliabue et al., 2014), which results in low mixed-layer Fe/PO_4 (Figures 4b and 5f). In contrast, upper mixed layers are richer in Fe in the North Atlantic subtropical gyre (Sedwick et al., 2005), which increases mixed-layer Fe/PO_4 throughout this region (Figure 5f). There is an increase in Fe/PO_4 in the western Atlantic around 35°S which is attributed to the offshore export of Fe-rich Brazilian shelf water (Rijkenberg et al., 2014).

Finally, mixed-layer Mn/PO_4 is relatively high throughout the tropics due to both the drawdown of PO_4 and enhanced mixed-layer Mn levels arising from dust input and maintenance of surface dissolved Mn by photoreduction (Figure 5g; Jickells et al., 2005; Mahowald et al., 2005; Sunda et al., 1983). The Mn/PO_4 ratio also decreases towards polar regions, and as this element is also elevated in low oxygen waters, it tends to exhibit an increasing availability in mixed layers overlying the western oxygen depleted zones (Figure 5g).

3.3.4. Ranking the Availability of Nutrient-Type and Scavenged-Type Resources

The variability in vertical profiles discussed in sections 3.1 and 3.2 generates a progressive transition from nutrient-type to scavenged-type profiles, which varies between resources. We use a correlation approach to rank each resource between two end-member resources: nutrient-type nitrate and scavenged-type manganese. The ranking is performed on the Atlantic integrated resource stocks in the winter mixed layer of each resource relative to phosphate, as phosphate is a well sampled macronutrient that avoids interactions with the nitrogen cycle (Figure 5). We then rank resource on a continuum between NO_3/PO_4 and Mn/PO_4, (Series [1], Table S1).

$$(\text{Nutrient type})\frac{NO_3}{PO_4}:\frac{Cd}{PO_4}:\frac{Si}{PO_4}:\frac{Zn}{PO_4}:\frac{Co}{PO_4}:\frac{Fe}{PO_4}:\frac{Mn}{PO_4}(\text{Scavenged type}) \quad [1]$$

The ranking in Series [1] reveals Cd/PO_4 is most comparable to NO_3/PO_4 for the full Atlantic data set, likely due to the noted similarities in the biogeochemical cycling of Cd and NO_3 (Bruland, 1980). Next in the series is Si/PO_4 and Zn/PO_4. The input of Si and Zn to the upper ocean from atmospheric deposition and rivers is analogous; further, both undergo remineralization deep in the water column and hence display comparable profiles (Bruland, 1980). Si and Zn are likely decoupled in Series [1] as reversible scavenging influences Zn only (Weber et al., 2018). Finally, Co/PO_4 and Fe/PO_4 are most similar to Mn/PO_4. Dust is a major input of Co, Fe, and Mn (Jickells et al., 2016) causing elevated surface concentrations akin to scavenged-type profiles; however, the trace elements are differentially sensitive to oxygen causing variations in the associated vertical profiles (Rijkenberg et al., 2012; Tagliabue et al., 2018; van Hulten et al., 2017).

The combination of (i) marked variability in the vertical profiles of different resources, (ii) resource-specific nutricline depths, and (iii) regional variations in the depth of winter mixing drives substantial variability in resource availability for marine microbes created across the Atlantic Ocean. This variability arises from the transition of different resources from exhibiting nutrient-like to scavenged-type variability and leads to the high latitudes being relatively replete in the nutrient-like elements NO_3, PO_4, Cd, Si, and Zn, and the low latitudes being relatively replete in Co, Fe, and Mn.

3.4. Vertical Entrainment of Resources

The vertical profiles of different resources and the covariance of the nutricline and winter mixing depth creates a range of different resource regimes. The vertical profiles of different resources and depth of seasonal mixing are used to calculate the flux of resources into the mixed layer in response to the entrainment of underlying waters. We acknowledge that there are physical supply mechanisms that operate in addition, but contend that the entrainment flux is likely to be predominant in many cases (Achterberg et al., 2018; Tagliabue et al., 2014; Williams & Follows 2003; Williams et al., 2000). In this analysis, a positive entrainment flux reflects an increase in mixed-layer resource concentration, while a negative entrainment flux reflects dilution of mixed-layer resource concentration.

3.4.1. NO_3, PO_4, and Cd Entrainment

The entrainment of NO_3 and PO_4 into the seasonal mixed layer varies over several orders of magnitude throughout the Atlantic Ocean. The largest NO_3 and PO_4 entrainment flux estimates are located in the North Atlantic subpolar gyre and along 40°S, >200 mmol NO_3 m^{-2} $year^{-1}$ and >100 mmol PO_4 m^{-2} $year^{-1}$ (Figures 6a and 6b). The diagnosed NO_3 and PO_4 fluxes here result from large property gradients in the vertical and the depth attained by winter mixing which exceeds the nutricline depth (Figures 3a, 3b, and 4a). In subtropical regions, the entrainment fluxes of NO_3 and PO_4 are greatly reduced (Figures 6a and 6b) as the winter mixing does not access the nitracline (Figures 3a and 4a). In regions of the high latitude Southern Ocean, the vertical entrainment of macronutrients is low (Figures 6a and 6b) despite high standing stocks (Figures 2a and 2b), which is because the vertical gradients of NO_3 and PO_4 are insufficient to drive a large macronutrient flux (Figures 2a, 2b, 6a, and 6b). The large-scale pattern in the entrainment flux of Cd is similar to that of NO_3 and PO_4, with maximum fluxes of >5 μmol m^{-2} $year^{-1}$ in high latitude regions. However, a small negative entrainment flux for Cd of ~ −0.001 to −0.005 μmol m^{-2} $year^{-1}$ occurs in some subtropical regions (Figure 6c) where there are slight increases in upper ocean Cd and the Cd nutricline is far deeper than the winter mixed-layer depth (Figure 3a).

3.4.2. Si and Zn Entrainment

The entrainment of Si is similar to that of other macronutrients NO_3 and PO_4, excluding the subtropical North Atlantic, with maximal values of >100 mmol m^{-2} $year^{-1}$ being widespread (Figure 6d). However, in the subtropical North Atlantic, the small subsurface minima in Si drives a small negative entrainment flux of −1 and −2 mmol m^{-2} $year^{-1}$. Here, mixed-layer Si becomes slightly diluted by the entrainment of relatively low Si waters from below. The entrainment of Zn into the mixed layer is largest in the North Atlantic subpolar gyre and around Drake Passage, where deep mixed layers access subsurface Zn stocks and cause entrainment fluxes of >50 μmol m^{-2} $year^{-1}$ (Figure 6e). Like Cd, the Zn entrainment flux in

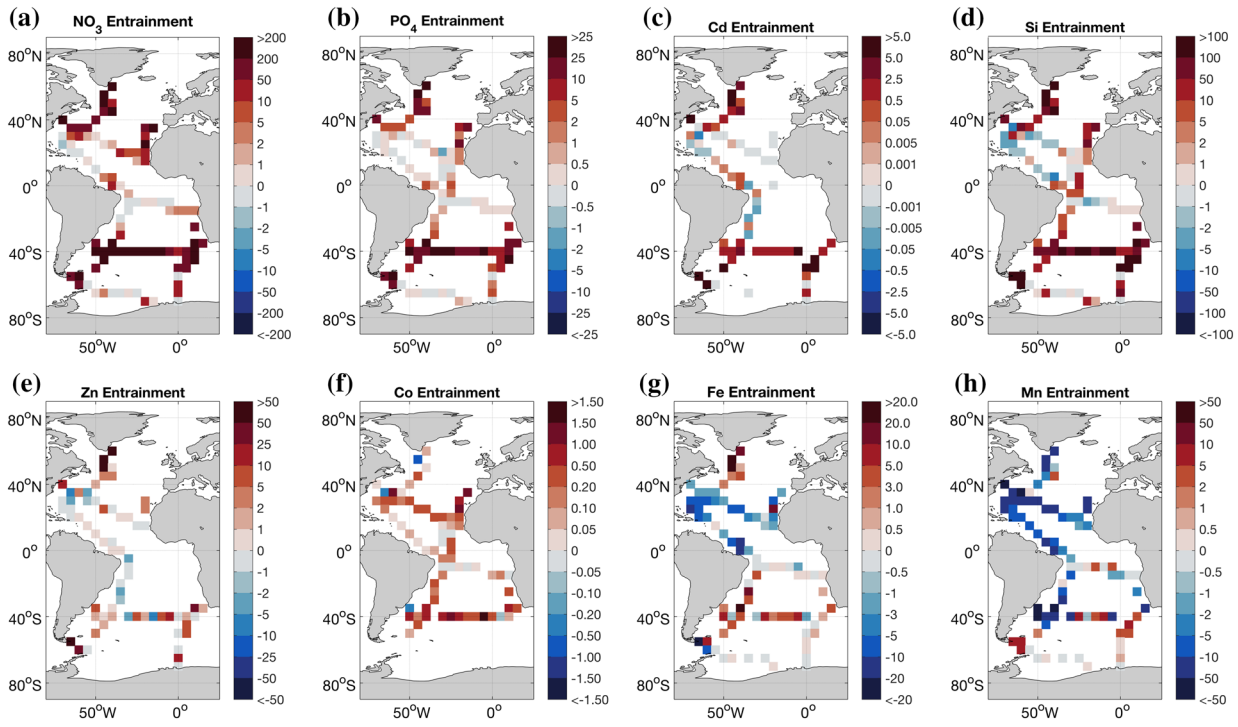

Figure 6. Entrainment flux of NO_3, PO_4, Si (all mmol m^{-2} $year^{-1}$), Cd, Zn, Fe, Co, and Mn (all μmol m^{-2} $year^{-1}$) to the Atlantic Ocean and Southern Ocean. Physical model data from ECCOv4r3 (Forget et al., 2015; Fukumori et al., 2017). Biogeochemical data from the 2017 *GEOTRACES* intermediate data product (Schlitzer et al., 2018).

the South Atlantic is negative, and both resources display a large offset between their respective nutricline depth and the winter mixed-layer depth (Figure S5b and S5c). Generally, the entrainment of Zn exhibits the greatest small-scale variability.

3.4.3. Co, Fe, and Mn Entrainment

Co exhibits a nutrient-type profile over the depths of seasonal mixing (Figure 2f) which drives a positive entrainment flux that reaches >1.5 μmol m^{-2} $year^{-1}$ the subtropical North Atlantic and along 40°S (Figure 6f). In the subtropical Atlantic, Co concentrations increase with depth to ~300 m due to underlying low oxygen waters, which elevates subsurface Co stocks and drives entrainment of around 0.5 μmol m^{-2} $year^{-1}$ (Figures 2f and 6f). Although the seasonal cycle of the mixed layer is large in the North Atlantic subpolar gyre, the vertical profile of Co is relatively uniform causing a very low entrainment flux of Co compared to that of other resources.

The entrainment flux of Fe reaches >10 μmol m^{-2} $year^{-1}$ in the North Atlantic subpolar gyre and along 40°S as winter mixing accesses subsurface Fe stocks (Figures 4b and 6g). In the Fe-limited Southern Ocean, the entrainment of Fe into the mixed layer is notably lower (~1–5 μmol m^{-2} $year^{-1}$) as the winter mixed-layer depth does reach subsurface iron stocks (Figures 4b and 6g). Seasonal entrainment acts to erode the mixed-layer Fe stock significantly in the subtropical North Atlantic, with dilution rates of >10 μmol m^{-2} $year^{-1}$ common for this region (Figure 6g). Similarly, the scavenged distribution of Mn causes seasonal entrainment to dilute mixed-layer Mn stocks by as much as 10–50 μmol m^{-2} $year^{-1}$ throughout much of the Atlantic (Figure 6h). There is a positive Mn entrainment flux of up to 10 nmol m^{-2} $year^{-1}$ in the Southern Ocean due to the combination of muted surface maxima and winter mixing crossing vertical Mn gradients (Figures 2h, 6h, and S5f).

4. Discussion

4.1. Biological Impacts of Variability in Resources Availability

The broad resource availability regimes identified in this study cause the deficiency of multiple resources throughout the Atlantic Ocean mixed layer. Deficiency may eventually lead to limitation as mixed-layer

resource stocks become exhausted during phytoplankton growth. For instance, in some regions, the winter mixed-layer NO_3/PO_4 ratio is 8 mol mol^{-1} (e.g., eastern subtropical South Atlantic, Figure 5a), which indicates a deficiency in NO_3 relative to PO_4 compared to Redfield 16N:1P (Redfield, 1934). The mixed layer shoals and biological uptake occurs at Redfield N:P, and the NO_3/PO_4 is reduced further as more NO_3 is removed than PO_4 compared to the original conditions. In this case, initial deficiency of NO_3 would lead to growth limitation by NO_3 assuming all other requirements are met. Growth limitation by NO_3 or Fe can be derived by a relationship between relative surface concentrations of NO_3 and Fe (Browning, Achterberg, Rapp, et al., 2017). If we apply this relationship to our winter mixed-layer resource stocks (rather than simply surface data), we find that 42% of individual locations are singularly limited by Fe, 25% exhibit Fe-N serial limitation, 14% display colimitation, 9% show N-Fe serial limitation, and 11% are singularly limited by N. The high latitude North Atlantic, Southern Ocean, and the Benguela upwelling region display signals of singular Fe limitation, while there is a small region of singular N-limitation in the North Atlantic subtropical gyre. Fe-N and N-Fe serial limitation, as well as Fe-N colimitation emerge as common features of the low latitude oceans (Figure S7). This indicates that variability in mixed-layer resource stocks (driven by vertical profiles and the depth of mixing) has the potential to drive large-scale patterns in nutrient (co) limitation.

Resource availability restricts productivity in the upper mixed layer, and microbial community structure may also be affected (Saito et al., 2015; Ward et al., 2013). For instance, when waters are deplete in NO_3, but replete in PO_4 and Fe, diazotrophs are able to exploit the N limitation of non-N fixing plankton and flourish (LaRoche & Breitbarth, 2005; Sohm et al., 2011; Ward et al., 2013). We find that such conditions arise in the east of the subtropical North Atlantic near the African coast, where NO_3/PO_4 decreases, indicating enhanced PO_4 supply and Fe stocks remain high (Figures 5a and 5f). This pattern agrees well with the distribution of diazotroph communities in the subtropical North Atlantic gyre (Ratten et al., 2015). Similarly, a database of diazotroph biomass (Luo et al., 2012) indicates high surface levels in the subtropical North Atlantic and between in 22.5°S and 37.5°S the western South Atlantic, which coincides with regions of low NO_3 and high Fe mixed-layer conditions we identified in this study (Figures 5a and 5f). The observed west to east transition from nanophytoplankton to picophytoplankton along 40°S (Browning et al., 2014) is coincident with a decline in Fe/PO_4, Zn/PO_4, Mn/PO_4, Cd/PO_4, and Co/PO_4 from west to east (Figure 5). New findings of diatoms in the subtropical North Atlantic (Lampe et al., 2019) are in agreement with elevated Si/PO_4 stocks we find in this region (Figure 5c). Overall, our results suggest that the broad resource regimes established in the Atlantic Ocean influence marine ecosystems.

While it is possible to link resource availability to the estimates of phytoplankton demand for various resources (e.g., Ho et al., 2003) to derive a "Redfield balance" (Redfield, 1934), doing so would ignore important interactions between trace elements, which dictates the interior physiology of marine phytoplankton (Sunda, 1989). For instance, new evidence suggests Zn and Mn can outcompete Co for a common uptake mechanism when Co is deficient, altering the link between resource availability and cellular accumulation (Hawco & Saito, 2018). In addition, the uptake of P from dissolved organic P at low PO_4 concentrations via alkaline phosphatase can be colimited by Zn and Fe (Browning, Achterberg, Yong, et al., 2017; Mahaffey et al., 2014; Shaked et al., 2006). Finally, many organisms adjust their biochemical apparatus under Fe stress, with for example, flavodoxin being produced instead of the Fe-containing ferredoxin (LaRoche et al., 1996) or the Cu-containing plastocyanin replacing the Fe-containing cytochrome b6 (Peers & Price, 2006). Moreover, Co and Zn are interchangeable in the carbon acquisition enzyme carbonic anhydrase (Sunda & Huntsman, 1995). In order to accurately diagnose the dominant limiting resource in a given region, we must develop our conceptual and theoretical understanding of trace metal interactions and account for the plasticity of phytoplankton interior stoichiometry instead of using fixed thresholds. In this context, expanding data sets of phytoplankton cell quotas (Finkel et al., 2006; Ho et al., 2003; Twining & Baines, 2013) and nutrient stress (Saito et al., 2014; Wu et al., 2019) would be invaluable in linking resource availability and demand.

4.2. Variability in the Winter Mixed Layer

The seasonal cycle of the mixed layer exhibits interannual variability (Holte et al., 2017) due to changes in physical controls (de Boyer Montegut et al., 2007) or climate modes (Sallee et al., 2010). It is possible that mixed-layer anomalies may markedly alter the growth environment due to the changes in the mixed-layer

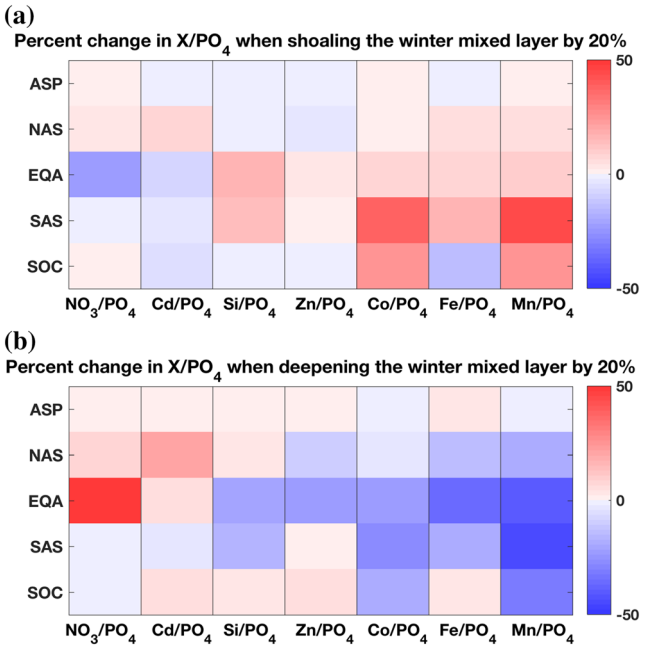

Figure 7. Biogeochemical province median percentage change in the elemental stoichiometry of resources in the winter mixed layer when the maximum annual mixed-layer depth is (a) shoaled and (b) deepened by 20%. Mixed-layer depth from ECCOv4r3 (Forget et al., 2015; Fukumori et al., 2017). Biogeochemical provinces are the Atlantic sub-polar gyre (ASP), North Atlantic sub-tropical (NAS), equatorial Atlantic (EQA), South Atlantic subtropical (SAS), and the Southern Ocean (SOC). An increase in X/PO_4 corresponds to an increase in the availability of X relative to PO_4 in the mixed layer compared to initial conditions. Ordered by nutrient type to scavenged type resource (see text). Biogeochemical data from the 2017 *GEOTRACES* Intermediate Data Product (Schlitzer et al., 2018).

resource availability (Barber & Chavez, 1983). To test this, we explored two different scenarios where the depth of the maximum annual mixed-layer depth was increased and decreased by a modest (5%) and large (20%) degree by altering the mixed-layer thickness (H) in equation (1) accordingly.

The integrated resource stocks decrease when the depth of winter mixing was reduced; however, there were notable fluctuations in relative stock of different resources (i.e., the ratio of a given resource to PO_4; Figures 7 and S8). Under both shoaling scenarios presented, decreasing the winter mixed-layer depth decreases NO_3/PO_4 in the equatorial Atlantic (Figures 7a and S8a). In the North and South Atlantic subtropical gyres, under the 5% shoaling case and the 20% shoaling case, opposing responses in mixed-layer NO_3/PO_4 occur as the NO_3 and PO_4 stoichiometry varies with depth (Figure S9). In the equatorial Atlantic and South Atlantic gyre, Si/PO_4, Zn/PO_4, Co/PO_4, Fe/PO_4, and Mn/PO_4 all increase alongside the decrease in NO_3/PO_4 and Cd/PO_4, implying Si and nonnutrient type trace elements become more abundant relative to NO_3, PO_4 and Cd under reduced winter mixing (Figure 7). In general, Si, Zn, and Fe all show greater availability relative to PO_4 at low latitudes and less availability relative to PO_4 in the most polar provinces. Co and Mn become more available everywhere relative to PO_4, excluding Fe in the Atlantic subpolar gyre. The changes under the 20% deepening scenario are generally opposite to those under the 20% shoaling scenario, deeper winter mixed layers lead to decreases in resource availability of Si, Zn, Co, Fe, and Mn relative to PO_4 in low latitude provinces. In some cases, shoaling and deepening drives the same response, which is attributed to gradients in the vertical profile of resource stoichiometries (Figure S9).

The effect of reducing the winter mixed-layer depth is likely to benefit nitrogen fixing diazotrophs in the equatorial Atlantic and South Atlantic gyre as NO_3/PO_4 is reduced while Fe/PO_4 increases, expanding the diazotroph niche (Ward et al., 2013). Additionally, increased Zn/PO_4 may promote alkaline phosphatase activity in these regions and alleviate PO_4 stress (Mahaffey et al., 2014). Overall, our results suggest that NO_3/PO_4 will increase in high latitudes while mid to low latitudes become richer in Si and nonnutrient type trace elements, allowing diazotrophs to thrive under reduced winter mixing, while the success of nondiazotrophs will be hampered.

4.3. Wider Considerations

4.3.1. Additional Resource Pathways to the Mixed Layer

The entrainment of resources into the mixed layer is augmented by additional supply pathways. Dust is a source of resources to the ocean surface (Jickells et al., 2005), and by combining typical modeled deposition rates (Duce et al., 2008; Mahowald et al., 2005), subtropical North Atlantic solubility measurements (Shelley et al., 2018), and crustal ratios (Rudnick & Gao, 2003), we estimate average annual dust fluxes of 9.9 ± 11.5 N, 0.02 ± 0.03 P, and 2.0 ± 4.1 Si (all mmol m^{-2} $year^{-1}$), $0.4 \pm 0.8 \times 10^{-3}$ Cd, 0.5 ± 1.0 Zn, 0.05 ± 0.11 Co, 50.0 ± 100.0 Fe, and 8.2 ± 16.3 Mn (all μmol m^{-2} $year^{-1}$) across all stations included in this study. The strongest dust influence is likely to be in the subtropical North Atlantic, where it may compensate for the loss of Fe and Mn from entrainment. However, as dust inputs of Fe and Mn are greater than the entrainment losses we estimate, it is likely that additional removal processes, such as scavenging and biological uptake, are operating on aerosol derived Fe and Mn. The minimal abundance of N and P in Earth's crust causes dust to be relatively depleted in N and P compared to Si, Fe, and Mn (Rudnick & Gao, 2003). N-fixation rates of up to 65 mmol N m^{-2} $year^{-1}$ have been observed in the subtropical North Atlantic (Moore et al., 2009), outweighing the entrainment input of N in this region (Figure 6a). Wind-driven Ekman transport in the North Atlantic may also provide up to 60 mmol N m^{-2} $year^{-1}$ on the northern flank of the subtropical gyre (Williams & Follows, 1998), comparable to our estimates of NO_3 entrainment in the same region. In the

north-western Atlantic, Gulf Stream rings have been suggested to deliver Fe to the subtropical gyre at a rate of 3.4 ± 1.9 μmol Fe m^{-2} $year^{-1}$ when averaged across the subtropical gyre area (Conway et al., 2018). This extra Fe would counter-act the estimated losses from entrainment of around −1 to −10 μmol Fe m^{-2} $year^{-1}$ in the region (Figure 6g). The comparison of entrainment with other physical supply pathways will vary across broad dynamical regimes. For example, in coastal or tropical regions upwelling is important; conversely, in downwelling regions such as subtropical gyres, entrainment will form a key pathway of resources to the euphotic zone (McGillicuddy, 2016). Additional physical process, such as horizontal advection (Palter et al., 2005) or mixing due to wind-driven internal waves (Whalen et al., 2018), operate alongside entrainment; however, we are unable to estimate their influence with the data sets used in this study. The external supply of resources to the winter mixed layer may alter the mixed-layer resource stoichiometry. Properly assessing the influence of the total external supply necessitates a complete understanding of each pathway.

4.3.2. Better Constraining Entrainment Estimates

Increased stratification may reduce winter mixed-layer depth, however; ocean warming may cause stronger thermal gradients to form (Rhein et al., 2013). This will increase the barrier presented by the main thermocline located between the surface mixed layer and deeper water, reducing the ventilation of the upper ocean (Frolicher et al., 2009). In such a scenario, the supply of resources to the mixed layer from diapycnal diffusion and upwelling is diminished, increasing the role of entrainment where nutriclines are located above the winter mixed-layer depth.

In order to better constrain the role of entrainment and future changes we require improved observational data coverage. In many high latitude systems (e.g., Southern Ocean), winter-time observations are scarce, affecting our estimates of the winter nutriclines and mixed-layer depths and subsequently entrainment at these locations. Monthly observations of resources, particularly when the mixed layer is deepening, are key to better constraining entrainment fluxes. In this study, we reconstruct winter profiles based on density structure rather than applying direct monthly observations. We require better understanding on how ocean warming will impact upper ocean physics, both spatially and temporally, as well as subsequent response in biogeochemical processes (e.g., remineralization depth). At present, there is little coherency in the projected changes to winter mixed-layer depths in models included in the Coupled Model Intercomparison Project—Phase 5 (CMIP5; Figure S10; Sallee et al., 2013; Taylor et al., 2012). To fully understand the future role of entrainment compared to other major sources, other factors such as atmospheric resource supplies should be considered (Mahowald & Luo, 2003).

5. Conclusions

This study synthesizes biogeochemical observational data with output from a physical ocean state estimation to determine basin-scale patterns in mixed-layer resource availability throughout the Atlantic Ocean. We find NO_3/PO_4 and Mn/PO_4 are endmembers displaying maxima in the high and low latitudes, respectively, due to their nutrient-like and scavenged-like characteristics. Cd/PO_4, Si/PO_4, Zn/PO_4, and Co/PO_4 tend to fall in between these two endmembers, while Fe/PO_4 shows different behavior in different regions of the Atlantic Ocean. These variations arise primarily due to the regional differences in the offset between the winter mixed-layer depth and the associated nutricline. When nutrient-type profiles prevail, the entrainment of thermocline waters into the mixed layer acts to alleviate deficiency of these resources. However, in regions where resources display scavenged-type profiles, then entrainment can cause a dilution of upper ocean stocks. This dilution occurs most prominently for Mn and Fe in the North Atlantic subtropical gyre and equatorial Atlantic and implies that the elevated upper ocean stocks must be sustained by other processes (e.g., dust deposition, lateral advection). Entrainment replenishes nutrient-type resources in the mixed layer and dilutes scavenged-type elements in the mixed layer. Future changes in the depth of winter-mixing will have a subsequent impact on mixed-layer resource availability. To link any change in the relative availability of various resources to phytoplankton growth requires a complete understanding of the stoichiometric plasticity and the colimitation of cellular processes, which is currently unavailable.

Acknowledgments

S. J. R. is supported by the Natural Environment Research Council (NERC) Earth, Atmosphere and Ocean Doctoral Training Partnership whose support is gratefully acknowledged (Grant NE/L002469/1). We thank GEOTRACES (www.geotraces.org) scientists involved in the collection, validation and processing of datasets used throughout this study. We acknowledge the ECCO group (www.ecco-group.org) for their continued model development and providing output files. S. J., R., A. T., and R. G. W. designed the research, while S. J. R. undertook the analysis with input from all coauthors. S. J. R. wrote the manuscript with the contribution of all coauthors. The authors declare no competing interests. All data used in this study are freely available online (subject to account creation): observational GEOTRACES data via the online service hosted at the Alfred Wenger Institute (https://webodv.awi.de/geotraces_extractor_bottle), Estimating the Circulation and Climate of the Ocean (ECCO) model output data hosted on the ECCO Drive (mixed-layer depth climatology at https://ecco.jpl.nasa.gov/drive/files/Version4/Release3/interp_climatology/MXLDEPTH.0001.nc, salinity climatology at https://ecco.jpl.nasa.gov/drive/files/Version4/Release3/interp_climatology/SALT.0001.nc, temperature climatology at https://ecco.jpl.nasa.gov/drive/files/Version4/Release3/interp_climatology/THETA.0001.nc), mixed-layer depth climatological output from models included in the fifth Coupled Model Intercomparison Project (CMIP5) are made available by the Earth System Grid Federation (https://esgf-node.llnl.gov/search/cmip5/). We thank Pete Morton and one anonymous reviewer for their helpful comments that have strengthened this manuscript.

References

Achterberg, E. P., Steigenberger, S., Marsay, C. M., LeMoigne, F. A. C., Painter, S. C., Baker, A. R., et al. (2018). Iron biogeochemistry in the high latitude North Atlantic Ocean. *Scientific Reports*, *8*(1), 1283. https://doi.org/10.1038/s41598-018-19472-1

Barber, R. T., & Chavez, F. P. (1983). Biological consequences of El-Nino. *Science*, *222*(4629), 1203–1210. https://doi.org/10.1126/science.222.4629.1203

Bopp, L., Monfray, P., Aumont, O., Dufresne, J. L., le Treut, H., Madec, G., et al. (2001). Potential impact of climate change on marine export production. *Global Biogeochemical Cycles*, *15*(1), 81–99. https://doi.org/10.1029/1999gb001256

Boye, M., Wake, B. D., Garcia, P. L., Bown, J., Baker, A. R., & Achterberg, E. P. (2012). Distributions of dissolved trace metals (Cd, Cu, Mn, Pb, Ag) in the southeastern Atlantic and the Southern Ocean. *Biogeosciences*, *9*(8), 3231–3246. https://doi.org/10.5194/bg-9-3231-2012

Browning, T. J., Achterberg, E. P., Rapp, I., Engel, A., Bertrand, E. M., Tagliabue, A., & Moore, C. M. (2017). Nutrient co-limitation at the boundary of an oceanic gyre. *Nature*, *551*(7679), 242. https://doi.org/10.1038/nature24063

Browning, T. J., Achterberg, E. P., Yong, J. C., Rapp, I., Utermann, C., Engel, A., & Moore, C. M. (2017). Iron limitation of microbial phosphorus acquisition in the tropical North Atlantic. *Nature Communications*, *8*, 15465. https://doi.org/10.1038/ncomms15465

Browning, T. J., Bouman, H. A., Moore, C. M., Schlosser, C., Tarran, G. A., Woodward, E. M. S., & Henderson, G. M. (2014). Nutrient regimes control phytoplankton ecophysiology in the South Atlantic. *Biogeosciences*, *11*(2), 463–479. https://doi.org/10.5194/bg-11-463-2014

Bruland, K. W. (1980). Oceanographic distributions of cadmium, zinc, nickel, and copper in the North Pacific. *Earth and Planetary Science Letters*, *47*(2), 176–198. https://doi.org/10.1016/0012-821x(80)90035-7

Conway, T. M., Hamilton, D. S., Shelley, R. U., Aguilar-Islas, A. M., Landing, W. M., Mahowald, N. M., & John, S. G. (2019). Tracing and constraining anthropogenic aerosol iron fluxes to the North Atlantic Ocean using iron isotopes. *Nature Communications*, *10*, 2628. https://doi.org/10.1038/s41467-019-10457-w

Conway, T. M., & John, S. G. (2014). The biogeochemical cycling of zinc and zinc isotopes in the North Atlantic Ocean. *Global Biogeochemical Cycles*, *28*, 1111–1128. https://doi.org/10.1002/2014gb004862

Conway, T. M., & John, S. G. (2015). Biogeochemical cycling of cadmium isotopes along a high-resolution section through the North Atlantic Ocean. *Geochimica et Cosmochimica Acta*, *148*, 269–283. https://doi.org/10.1016/j.gca.2014.09.032

Conway, T. M., Palter, J. B., & de Souza, G. F. (2018). Gulf Stream rings as a source of iron to the North Atlantic subtropical gyre. *Nature Geoscience*, *11*(8), 594. https://doi.org/10.1038/s41561-018-0162-0

Croot, P. L., Baars, O., & Streu, P. (2011). The distribution of dissolved zinc in the Atlantic sector of the Southern Ocean. *Deep-Sea Research Part Ii-Topical Studies in Oceanography*, *58*(25–26), 2707–2719. https://doi.org/10.1016/j.dsr2.2010.10.041

de Boyer Montegut, C., Vialard, J., Shenoi, S. S. C., Shankar, D., Durand, F., Ethe, C., & Madec, G. (2007). Simulated seasonal and interannual variability of the mixed layer heat budget in the northern Indian Ocean. *Journal of Climate*, *20*(13), 3249–3268. https://doi.org/10.1175/Jcli4148.1

Duce, R. A., LaRoche, J., Altieri, K., Arrigo, K. R., Baker, A. R., Capone, D. G., et al. (2008). Impacts of atmospheric anthropogenic nitrogen on the open ocean. *Science*, *320*(5878), 893–897. https://doi.org/10.1126/science.1150369

Dulaquais, G., Boye, M., Rijkenberg, M. J. A., & Carton, X. (2014). Physical and remineralization processes govern the cobalt distribution in the deep western Atlantic Ocean. *Biogeosciences*, *11*(6), 1561–1580. https://doi.org/10.5194/bg-11-1561-2014

Falkowski, P. G., Barber, R. T., & Smetacek, V. (1998). Biogeochemical controls and feedbacks on ocean primary production. *Science*, *281*(5374), 200–206. https://doi.org/10.1126/science.281.5374.200

Finkel, Z. V., Quigg, A., Raven, J. A., Reinfelder, J. R., Schofield, O. E., & Falkowski, P. G. (2006). Irradiance and the elemental stoichiometry of marine phytoplankton. *Limnology and Oceanography*, *51*(6), 2690–2701. https://doi.org/10.4319/lo.2006.51.6.2690

Forget, G., Campin, J. M., Heimbach, P., Hill, C. N., Ponte, R. M., & Wunsch, C. (2015). ECCO version 4: An integrated framework for non-linear inverse modeling and global ocean state estimation. *Geoscientific Model Development*, *8*(10), 3071–3104. https://doi.org/10.5194/gmd-8-3071-2015

Frolicher, T. L., Joos, F., Plattner, G. K., Steinacher, M., & Doney, S. C. (2009). Natural variability and anthropogenic trends in oceanic oxygen in a coupled carbon cycle-climate model ensemble. *Global Biogeochemical Cycles*, *23*, GB1003. https://doi.org/10.1029/2008gb003316

Fukumori, I., Wang, O., Fenty, I., Forget, G., Heimbach, P., & Ponte, R. M. (2017). ECCO Version 4 Release 3, http://hdl.handle.net/1721.1/110380. http://1721.1/110380 Retrieved from ftp://ecco.jpl.nasa.gov/Version4/Release3/doc/v4r3_estimation_synopsis.pdf

Hatta, M., Measures, C. I., Wu, J. F., Roshan, S., Fitzsimmons, J. N., Sedwick, P., & Morton, P. (2015). An overview of dissolved Fe and Mn distributions during the 2010–2011 US GEOTRACES north Atlantic cruises: GEOTRACES GA03. *Deep-Sea Research Part Ii-Topical Studies in Oceanography*, *116*, 117–129. https://doi.org/10.1016/j.dsr2.2014.07.005

Hawco, N. J., Ohnemus, D. C., Resing, J. A., Twining, B. S., & Saito, M. A. (2016). A dissolved cobalt plume in the oxygen minimum zone of the eastern tropical South Pacific. *Biogeosciences*, *13*(20), 5697–5717. https://doi.org/10.5194/bg-13-5697-2016

Hawco, N. J., & Saito, M. A. (2018). Competitive inhibition of cobalt uptake by zinc and manganese in a pacific Prochlorococcus strain: Insights into metal homeostasis in a streamlined oligotrophic cyanobacterium. *Limnology and Oceanography*, *63*(5), 2229–2249. https://doi.org/10.1002/lno.10935

Ho, T. Y., Quigg, A., Finkel, Z. V., Milligan, A. J., Wyman, K., Falkowski, P. G., & Morel, F. M. M. (2003). The elemental composition of some marine phytoplankton. *Journal of Phycology*, *39*(6), 1145–1159. https://doi.org/10.1111/j.0022-3646.2003.03-090.x

Holte, J., Talley, L. D., Gilson, J., & Roemmich, D. (2017). An Argo mixed layer climatology and database. *Geophysical Research Letters*, *44*, 5618–5626. https://doi.org/10.1002/2017gl073426

Holzer, M., Primeau, F. W., DeVries, T., & Matear, R. (2014). The Southern Ocean silicon trap: Data-constrained estimates of regenerated silicic acid, trapping efficiencies, and global transport paths. *Journal of Geophysical Research: Oceans*, *119*, 313–331. https://doi.org/10.1002/2013jc009356

Jickells, T. D., An, Z. S., Andersen, K. K., Baker, A. R., Bergametti, G., Brooks, N., et al. (2005). Global iron connections between desert dust, ocean biogeochemistry, and climate. *Science*, *308*(5718), 67–71. https://doi.org/10.1126/science.1105959

Jickells, T. D., Baker, A. R., & Chance, R. (2016). Atmospheric transport of trace elements and nutrients to the oceans. *Philosophical Transactions of the Royal Society a-Mathematical Physical and Engineering Sciences*, *374*(2081). https://doi.org/10.1098/rsta.2015.0286

Klunder, M. B., Laan, P., Middag, R., de Baar, H. J. W., & van Ooijen, J. C. (2011). Dissolved iron in the Southern Ocean (Atlantic sector). *Deep-Sea Research Part Ii-Topical Studies in Oceanography*, *58*(25–26), 2678–2694. https://doi.org/10.1016/j.dsr2.2010.10.042

Kraus, E. B., & Turner, J. S. (1967). A one-dimensional model of easonal thermocline.2. General theory and its consequences. *Tellus*, *19*(1), 98.

Lampe, R. H., Wang, S., Cassar, N., & Marchetti, A. (2019). Strategies among phytoplankton in response to alleviation of nutrient stress in a subtropical gyre. *The ISME Journal*, *13*(12), 2984–2997. https://doi.org/10.1038/s41396-019-0489-6

LaRoche, J., Boyd, P. W., McKay, R. M. L., & Geider, R. J. (1996). Flavodoxin as an in situ marker for iron stress in phytoplankton. *Nature*, *382*(6594), 802–805.

LaRoche, J., & Breitbarth, E. (2005). Importance of the diazotrophs as a source of new nitrogen in the ocean. *Journal of Sea Research*, *53*(1–2), 67–91. https://doi.org/10.1016/j.seares.2004.05.005
Longhurst, A. R. (2007). *Ecological geography of the sea*, ((2nd ed.). Amsterdam; Boston, MA: Academic Press.
Ludwig, M. L., & Matthews, R. G. (1997). Structure-based perspectives on B-12-dependent enzymes. *Annual Review of Biochemistry*, *66*, 269–313. https://doi.org/10.1146/annurev.biochem.66.1.269
Luo, Y. W., Doney, S. C., Anderson, L. A., Benavides, M., Berman-Frank, I., Bode, A., et al. (2012). Database of diazotrophs in global ocean: Abundance, biomass and nitrogen fixation rates. *Earth System Science Data*, *4*(1), 47–73. https://doi.org/10.5194/essd-4-47-2012
Mahaffey, C., Reynolds, S., Davis, C. E., & Lohan, M. C. (2014). Alkaline phosphatase activity in the subtropical ocean: insights from nutrient, dust and trace metal addition experiments. *Frontiers in Marine Science*, *1*(73). https://doi.org/10.3389/fmars.2014.00073
Mahowald, N. M., Baker, A. R., Bergametti, G., Brooks, N., Duce, R. A., Jickells, T. D., et al. (2005). Atmospheric global dust cycle and iron inputs to the ocean. *Global Biogeochemical Cycles*, *19*, GB4025. https://doi.org/10.1029/2004gb002402
Mahowald, N. M., & Luo, C. (2003). A less dusty future? *Geophysical Research Letters*, *30*(17), 1903. https://doi.org/10.1029/2003gl017880
Marra, J., Bidigare, R. R., & Dickey, T. D. (1990). Nutrients and mixing, chlorophyll and phytoplankton growth. *Deep-Sea Research Part a-Oceanographic Research Papers*, *37*(1), 127–143. https://doi.org/10.1016/0198-0149(90)90032-Q
Martin, A. P., Lucas, M. I., Painter, S. C., Pidcock, R., Prandke, H., Prandke, H., & Stinchcombe, M. C. (2010). The supply of nutrients due to vertical turbulent mixing: A study at the Porcupine Abyssal Plain study site in the northeast Atlantic. *Deep-Sea Research Part Ii-Topical Studies in Oceanography*, *57*(15), 1293–1302. https://doi.org/10.1016/j.dsr2.2010.01.006
Martin, J. H., & Fitzwater, S. E. (1988). Iron-deficiency limits phytoplankton growth in the Northeast Pacific Subarctic. *Nature*, *331*(6154), 341–343. https://doi.org/10.1038/331341a0
McGillicuddy, D. J. (2016). Mechanisms of physical-biological-biogeochemical interaction at the oceanic mesoscale. *Annual Review of Marine Science*, *8*(1), 125–159. https://doi.org/10.1146/annurev-marine-010814-015606
Middag, R., de Baar, H. J. W., & Bruland, K. W. (2019). The relationships between dissolved zinc and major nutrients phosphate and silicate along the GEOTRACES GA02 transect in the West Atlantic Ocean. *Global Biogeochemical Cycles*, *33*, 63–84. https://doi.org/10.1029/2018gb006034
Middag, R., de Baar, H. J. W., Laan, P., Cai, P. H., & van Ooijen, J. C. (2011). Dissolved manganese in the Atlantic sector of the Southern Ocean. *Deep-Sea Research Part Ii-Topical Studies in Oceanography*, *58*(25–26), 2661–2677. https://doi.org/10.1016/j.dsr2.2010.10.043
Middag, R., van Heuven, S. M. A. C., Bruland, K. W., & de Baar, H. J. W. (2018). The relationship between cadmium and phosphate in the Atlantic Ocean unravelled. *Earth and Planetary Science Letters*, *492*, 79–88. https://doi.org/10.1016/j.epsl.2018.03.046
Mills, M. M., Ridame, C., Davey, M., La Roche, J., & Geider, R. J. (2004). Iron and phosphorus co-limit nitrogen fixation in the eastern tropical North Atlantic. *Nature*, *429*(6989), 292–294. https://doi.org/10.1038/nature02550
Moore, C. M. (2016). Diagnosing oceanic nutrient deficiency. *Philosophical Transactions of the Royal Society a-Mathematical Physical and Engineering Sciences*, *374*(2081). https://doi.org/10.1098/rsta.2015.0290
Moore, C. M., Mills, M. M., Achterberg, E. P., Geider, R. J., LaRoche, J., Lucas, M. I., et al. (2009). Large-scale distribution of Atlantic nitrogen fixation controlled by iron availability. *Nature Geoscience*, *2*(12), 867–871. https://doi.org/10.1038/ngeo667
Moore, C. M., Mills, M. M., Arrigo, K. R., Berman-Frank, I., Bopp, L., Boyd, P. W., et al. (2013). Processes and patterns of oceanic nutrient limitation. *Nature Geoscience*, *6*(9), 701–710. https://doi.org/10.1038/Ngeo1765
Morel, F. M. M., & Price, N. M. (2003). The biogeochemical cycles of trace metals in the oceans. *Science*, *300*(5621), 944–947. https://doi.org/10.1126/science.1083545
Nielsdottir, M. C., Moore, C. M., Sanders, R., Hinz, D. J., & Achterberg, E. P. (2009). Iron limitation of the postbloom phytoplankton communities in the Iceland Basin. *Global Biogeochemical Cycles*, *23*, GB3001. https://doi.org/10.1029/2008gb003410
Noble, A. E., Lamborg, C. H., Ohnemus, D. C., Lam, P. J., Goepfert, T. J., Measures, C. I., et al. (2012). Basin-scale inputs of cobalt, iron, and manganese from the Benguela-Angola front to the South Atlantic Ocean. *Limnology and Oceanography*, *57*(4), 989–1010. https://doi.org/10.4319/lo.2012.57.4.0989
Okin, G. S., Baker, A. R., Tegen, I., Mahowald, N. M., Dentener, F. J., Duce, R. A., et al. (2011). Impacts of atmospheric nutrient deposition on marine productivity: Roles of nitrogen, phosphorus, and iron. *Global Biogeochemical Cycles*, *25*, GB2022. https://doi.org/10.1029/2010gb003858
Omand, M. M., & Mahadevan, A. (2015). The shape of the oceanic nitracline. *Biogeosciences*, *12*(11), 3273–3287. https://doi.org/10.5194/bg-12-3273-2015
Oschlies, A. (2002). Nutrient supply to the surface waters of the North Atlantic: A model study. *Journal of Geophysical Research*, *107*(C5), 3046. https://doi.org/10.1029/2000jc000275
Painter, S. C., Henson, S. A., Forryan, A., Steigenberger, S., Klar, J., Stinchcombe, M. C., et al. (2014). An assessment of the vertical diffusive flux of iron and other nutrients to the surface waters of the subpolar North Atlantic Ocean. *Biogeosciences*, *11*(8), 2113–2130. https://doi.org/10.5194/bg-11-2113-2014
Palter, J. B., Lozier, M. S., & Barber, R. T. (2005). The effect of advection on the nutrient reservoir in the North Atlantic subtropical gyre. *Nature*, *437*(7059), 687–692. https://doi.org/10.1038/nature03969
Peers, G., & Price, N. M. (2006). Copper-containing plastocyanin used for electron transport by an oceanic diatom. *Nature*, *441*(7091), 341–344. https://doi.org/10.1038/nature04630
Prince, N. M., & Morel, F. M. M. (1990). Cadmium and cobalt substitution for zinc in a marine diatom. *Nature*, *344*, 658–660.
Ratten, J. M., LaRoche, J., Desai, D. K., Shelley, R. U., Landing, W. M., Boyle, E., et al. (2015). Sources of iron and phosphate affect the distribution of diazotrophs in the North Atlantic. *Deep-Sea Research Part Ii-Topical Studies in Oceanography*, *116*, 332–341. https://doi.org/10.1016/j.dsr2.2014.11.012
Redfield, A. (1934). On the properties of organic derivatives in sea water and their relation to the composition of phytoplankton. In R. J. Daniel (ed.), *James Johnstone memorial volume* (pp. 177–192). Liverpool, UK: University Press of Liverpool.
Rhein, M., Rintoul, S. R., Aoki, S., Campos, E., Chambers, D., Feely, R. A., et al. (2013). Observations: Ocean. In T. F. Stocker, D. Qin, G.-K. Plattner, M. Tignor, S. K. Allen, J. Boschung, A. Nauels, Y. Xia, V. Bex, & P. M. Midgley (Eds.), *Climate Change 2013: The Physical Science Basis. Contribution of Working Group I to the Fifth Assessment Report of the Intergovernmental Panel on Climate Change* (pp. 255–316). Cambridge, United Kingdom and New York, NY, USA: Cambridge University Press.
Rijkenberg, M. J. A., Middag, R., Laan, P., Gerringa, L. J. A., van Aken, H. M., Schoemann, V., et al. (2014). The distribution of dissolved iron in the West Atlantic Ocean. *PLoS ONE*, *9*(6), e101323. https://doi.org/10.1371/journal.pone.0101323
Rijkenberg, M. J. A., Steigenberger, S., Powell, C. F., van Haren, H., Patey, M. D., Baker, A. R., & Achterberg, E. P. (2012). Fluxes and distribution of dissolved iron in the eastern (sub-) tropical North Atlantic Ocean. *Global Biogeochemical Cycles*, *26*, GB3004. https://doi.org/10.1029/2011gb004264

Rodionov, D. A., Vitreschak, A. G., Mironov, A. A., & Gelfand, M. S. (2003). Comparative genomics of the vitamin B-12 metabolism and regulation in prokaryotes. *Journal of Biological Chemistry*, *278*(42), 41148–41159. https://doi.org/10.1074/jbc.M305837200

Rudnick, R. L., & Gao, S. (2003). Composition of the continental crust. In H. D. Holland, & K. K. Turekian (Eds.), *Treatise on Geochemistry* (pp. 1–64). Oxford, UK: Elsevier.

Saito, M. A., McIlvin, M. R., Moran, D. M., Goepfert, T. J., DiTullio, G. R., Post, A. F., & Lamborg, C. H. (2014). Multiple nutrient stresses at intersecting Pacific Ocean biomes detected by protein biomarkers. *Science*, *345*(6201), 1173–1177. https://doi.org/10.1126/science.1256450

Saito, M. A., McIlvin, M. R., Moran, D. M., Goepfert, T. J., DiTullio, G. R., Post, A. F., & Lamborg, C. H. (2015). Multiple nutrient stresses at intersecting Pacific Ocean biomes detected by protein biomarkers (vol 345, 1173, 2014). *Science*, *347*(6221). https://doi.org/10.1126/science.aaa7328

Sallee, J. B., Shuckburgh, E., Bruneau, N., Meijers, A. J. S., Bracegirdle, T. J., Wang, Z., & Roy, T. (2013). Assessment of Southern Ocean water mass circulation and characteristics in CMIP5 models: Historical bias and forcing response. *Journal of Geophysical Research: Oceans*, *118*, 1830–1844. https://doi.org/10.1002/jgrc.20135

Sallee, J. B., Speer, K. G., & Rintoul, S. R. (2010). Zonally asymmetric response of the Southern Ocean mixed-layer depth to the Southern Annular Mode. *Nature Geoscience*, *3*(4), 273–279. https://doi.org/10.1038/Ngeo812

Sarmiento, J. L., Gruber, N., Brzezinski, M. A., & Dunne, J. P. (2004). High-latitude controls of thermocline nutrients and low latitude biological productivity. *Nature*, *427*(6969), 56–60. https://doi.org/10.1038/nature02127

Schlitzer, R., Anderson, R. F., Dodas, E. M., Lohan, M., Geibere, W., Tagliabue, A., et al. (2018). The GEOTRACES Intermediate Data Product 2017. *Chemical Geology*, *493*, 210–223. https://doi.org/10.1016/j.chemgeo.2018.05.040

Sedwick, P. N., Church, T. M., Bowie, A. R., Marsay, C. M., Ussher, S. J., Achilles, K. M., et al. (2005). Iron in the Sargasso Sea (Bermuda Atlantic Time-series Study region) during summer: Eolian imprint, spatiotemporal variability, and ecological implications. *Global Biogeochemical Cycles*, *19*, GB4006. https://doi.org/10.1029/2004gb002445

Sen Gupta, A., Santoso, A., Taschetto, A. S., Ummenhofer, C. C., Trevena, J., & England, M. H. (2009). Projected Changes to the Southern Hemisphere Ocean and Sea Ice in the IPCC AR4 Climate Models. *Journal of Climate*, *22*(11), 3047–3078.https://doi.org/10.1175/2008jcli2827.1

Shaked, Y., Xu, Y., Leblanc, K., & Morel, F. M. M. (2006). Zinc availability and alkaline phosphatase activity in Emiliania huxleyi: Implications for Zn-P co-limitation in the ocean. *Limnology and Oceanography*, *51*(1), 299–309. https://doi.org/10.4319/lo.2006.51.1.0299

Shelley, R. U., Landing, W. M., Ussher, S. J., Planquette, H., & Sarthou, G. (2018). Regional trends in the fractional solubility of Fe and other metals from North Atlantic aerosols (GEOTRACES cruises GA01 and GA03) following a two-stage leach. *Biogeosciences*, *15*(7), 2271–2288. https://doi.org/10.5194/bg-15-2271-2018

Sohm, J. A., Webb, E. A., & Capone, D. G. (2011). Emerging patterns of marine nitrogen fixation. *Nature Reviews Microbiology*, *9*(7), 499–508. https://doi.org/10.1038/nrmicro2594

Sunda, W. G. (1989). Trace metal interactions with marine phytoplankton. *Biological Oceanography*, *6*(5–6), 411–442.

Sunda, W. G., & Huntsman, S. A. (1995). Cobalt and zinc interreplacement in marine phytoplankton: Biological and geochemical implications. *Limnology and Oceanography*, *40*(8), 1404–1417. https://doi.org/10.4319/lo.1995.40.8.1404

Sunda, W. G., Huntsman, S. A., & Harvey, G. R. (1983). Photo-reduction of manganese oxides in seawater and its geochemical and biological implications. *Nature*, *301*(5897), 234–236. https://doi.org/10.1038/301234a0

Tagliabue, A. (2019). Elemental Distribution: Overview. In J. K. Cochran, H. J. Bokuniewicz, & P. L. Yager (Eds.), *Encyclopedia of Ocean Sciences* (3rd ed., Vol. 1, pp. 122–127). London: Elsevier.

Tagliabue, A., Hawco, N. J., Bundy, R. M., Landing, W. M., Milne, A., Morton, P. L., & Saito, M. A. (2018). The role of external inputs and internal cycling in shaping the global ocean cobalt distribution: Insights from the first cobalt biogeochemical model. *Global Biogeochemical Cycles*, *32*, 594–616. https://doi.org/10.1002/2017gb005830

Tagliabue, A., Sallee, J. B., Bowie, A. R., Levy, M., Swart, S., & Boyd, P. W. (2014). Surface-water iron supplies in the Southern Ocean sustained by deep winter mixing. *Nature Geoscience*, *7*(4), 314–320. https://doi.org/10.1038/Ngeo2101

Taylor, K. E., Stouffer, R. J., & Meehl, G. A. (2012). An overview of Cmip5 and the experiment design. *Bulletin of the American Meteorological Society*, *93*(4), 485–498. https://doi.org/10.1175/Bams-D-11-00094.1

Tuerena, R. E., Ganeshram, R. S., Geibert, W., Fallick, A. E., Dougans, J., Tait, A., et al. (2015). Nutrient cycling in the Atlantic basin: The evolution of nitrate isotope signatures in water masses. *Global Biogeochemical Cycles*, *29*, 1830–1844. https://doi.org/10.1002/2015gb005164

Tuerena, R. E., Williams, R. G., Mahaffey, C., Vic, C., Green, J. A. M., Naveira-Garabato, A., et al. (2019). Internal tides drive nutrient fluxes into the deep chlorophyll maximum over mid-ocean ridges. *Global Biogeochemical Cycles*, *33*, 995–1009. https://doi.org/10.1029/2019gb006214

Twining, B. S., & Baines, S. B. (2013). The trace metal composition of marine phytoplankton. *Annual Review of Marine Science*, *5*(5), 191–215. https://doi.org/10.1146/annurev-marine-121211-172322

Twining, B. S., Nodder, S. D., King, A. L., Hutchins, D. A., LeCleir, G. R., DeBruyn, J. M., et al. (2014). Differential remineralization of major and trace elements in sinking diatoms. *Limnology and Oceanography*, *59*(3), 689–704. https://doi.org/10.4319/lo.2014.59.3.0689

Twining, B. S., Rauschenberg, S., Morton, P. L., & Vogt, S. (2015). Metal contents of phytoplankton and labile particulate material in the North Atlantic Ocean. *Progress in Oceanography*, *137*, 261–283. https://doi.org/10.1016/j.pocean.2015.07.001

van Hulten, M., Middag, R., Dutay, J. C., de Baar, H., Roy-Barman, M., Gehlen, M., et al. (2017). Manganese in the west Atlantic Ocean in the context of the first global ocean circulation model of manganese. *Biogeosciences*, *14*(5), 1123–1152. https://doi.org/10.5194/bg-14-1123-2017

Ward, B. A., Dutkiewicz, S., Moore, C. M., & Follows, M. J. (2013). Iron, phosphorus, and nitrogen supply ratios define the biogeography of nitrogen fixation. *Limnology and Oceanography*, *58*(6), 2059–2075. https://doi.org/10.4319/lo.2013.58.6.2059

Weber, T., John, S., Tagliabue, A., & DeVries, T. (2018). Biological uptake and reversible scavenging of zinc in the global ocean. *Science*, *361*(6397), 73. https://doi.org/10.1126/science.aap8532

Whalen, C. B., MacKinnon, J. A., & Talley, L. D. (2018). Large-scale impacts of the mesoscale environment on mixing from wind-driven internal waves. *Nature Geoscience*, *11*(11), 842. https://doi.org/10.1038/s41561-018-0213-6

Williams, R. G., & Follows, M. J. (1998). The Ekman transfer of nutrients and maintenance of new production over the North Atlantic. *Deep-Sea Research Part I-Oceanographic Research Papers*, *45*(2–3), 461–489. https://doi.org/10.1016/S0967-0637(97)00094-0

Williams, R. G., & Follows, M. J. (2003). In M. J. R. Fasham (Ed.), *Physical transport of nutrients and the maintenance of biological production*. New York: Springer-Verlag.

Williams, R. G., McLaren, A. J., & Follows, M. J. (2000). Estimating the convective supply of nitrate and implied variability in export production over the North Atlantic. *Global Biogeochemical Cycles*, *14*(4), 1299–1313. https://doi.org/10.1029/2000gb001260

Williams, R. G., Roussenov, V., & Follows, M. J. (2006). Nutrient streams and their induction into the mixed layer. *Global Biogeochemical Cycles*, *20*, GB1016. https://doi.org/10.1029/2005gb002586

Wu, M., McCain, J. S. P., Rowland, E., Middag, R., Sandgren, M., Allen, A. E., & Bertrand, E. M. (2019). Manganese and iron deficiency in Southern Ocean Phaeocystis antarctica populations revealed through taxon-specific protein indicators. *Nature Communications*, *10*, 3582. https://doi.org/10.1038/s41467-019-11426-z

Wyatt, N. J., Milne, A., Woodward, E. M. S., Rees, A. P., Browning, T. J., Bouman, H. A., et al. (2014). Biogeochemical cycling of dissolved zinc along the GEOTRACES South Atlantic transect GA10 at 40 S. *Global Biogeochemical Cycles*, *28*, 44–56. https://doi.org/10.1002/2013gb004637